Anatase Coarsening Kinetics under Hydrothermal Conditions As a Function of Ph and Temperature

Michael P. Finnegan,* Hengzhong Zhang,* and Jillian F. Banfield

Department of Earth and Planetary Sciences, McCone Hall, University of California, Berkeley, California 94720-4767

Received April 18, 2007. Revised Manuscript Received February 13, 2008

Nanoparticles coarsen in solution via atom-by-atom dissolution and reattachment (Ostwald ripening) or via crystallographically controlled attachment of discrete particles (oriented attachment). We coarsened anatase nanoparticles in hydrothermal solutions over the temperature range 105−250 °C and the pH range 1−12 and documented three distinct coarsening mechanisms controlled by solution pH. Anatase growth at pH > 11 occurs primarily by Ostwald ripening, yielding a wide particle size distribution. Over the pH range of 2 through 11, anatase grows both by oriented attachment and Ostwald ripening. At pH values <2, anatase simultaneously grows by oriented attachment and dissolves, precipitating as rutile. Oriented attachment is significant at values nearer to the pH of point of zero net proton charge (PZC), where anatase is very insoluble and has low surface charge. Rutile precipitation at low pH and anatase growth at high pH are promoted by enhanced Ti solubility at pH values far from the PZC. Understanding solution pH effects on assembly and coarsening kinetics may enable improved control of nanoparticle properties.

Introduction

Nanometer-scale materials are prevalent in the natural environment and find uses in an increasing number of technological applications.[1–4] The coarsening of nanoparticles changes the surface defect concentration, surface energy, and cumulative surface area.[5] Such changes can profoundly affect the rate and mechanism of nanoparticle transport, as well as the surface reactivity and adsorption capacity of nanoparticles. Thus, the impact of nanoparticles in natural aqueous and atmospheric environments will be partly determined by size.[6,7] Furthermore, the unintended coarsening of nanoparticles may result in reduced performance in technological applications. For example, the size of anatase nanoparticles affects the power output of dye-sensitized TiO_2 solar cells by increasing the effective area of the diode.[8] Even the morphology can affect the power output as different crystallographic surfaces perform differently as solar cell electrodes.[9] Similarly, the effectiveness of TiO_2 photocatalysis for photodegradation of noxious species in aqueous medium is partially controlled by the particle size.[10] Furthermore, the impact of particle size on materials properties such as piezoelectricity, surface reactivity, magnetism, and ductility has been documented.[11,12]

Classical descriptions of particle growth are based on the concept of Ostwald ripening (OR), which involves dissolution of small particles and growth of larger particles at a rate that is directly proportional to the solid's solubility and solid–liquid interfacial tension, and affected by particle size distribution.[13–15] Oriented attachment (OA) is an alternative growth pathway in which larger crystals form by crystallographically controlled assembly of smaller nanocrystals.[16] Particles approach each other and attach on crystallographic matching terminating surfaces. Atom by atom surface diffusion may ensue, eliminating topographic roughness.

OA growth has been documented in TiO_2 by Penn and Banfield,[16] in SnO_2 by Leite et al.,[17] in FeOOH by Banfield

* To whom correspondence should be addressed. Address: Materials Science Program, University of Wisconsin, Madison, WI. E-mail: m.p.finnegan@gmail.com. Phone: (510) 841-4150.

(1) Banfield, J. F.; Zhang, H. Z. In *Reviews in Mineralogy & Geochmistry; Nanoparticles and the Environment*; Banfield, J. F., Navrotsky, A. , Eds.; Mineralogical Society of America: Chantilly, VA, 2001; Vol. 44, pp 1–51.
(2) Park, N. G.; van de Lagemaat, J.; Frank, A. J. *J. Phys. Chem. B* **2000**, *104* (38), 8989–8994.
(3) Gratzel, M. *Proc.— Indian Acad. Sci., Chem. Sci.* **1995**, *107* (6), 607–619.
(4) Ganguli, A. K.; Jha, P.; Ahmad, T.; Arya, P. R. *Indian J. Phys. Proc. Indian Assoc. Cultivation Sci., Part A* **2004**, *78A* (1), 13–17.
(5) Baraton, M. I.; Merhari, L. *J. Nano. Res.* **2004**, *6* (1), 107–117.
(6) Yariv, S.; Cross, H. *Geochemistry of Colloid Systems*; Springer-Verlag: New York, 1979; p p242–244.
(7) Zhang, H. Z.; Penn, R. L.; Hamers, R. J.; Banfield, J. F. *J. Phys. Chem. B.* **1999**, *103* (22), 4656–4662.
(8) Park, N. G.; Schlichtorl, G.; van de Lagemaat, J.; Cheong, H. M.; Mascarenhas, A.; Frank, A. J. *J. Phys. Chem. B* **1999**, *103* (17), 3308–3314.
(9) Zaban, A.; Aruna, S. T.; Tirosh, S.; Gregg, B. A.; Mastai, Y. *J. Phys. Chem. B* **2000**, *104* (17), 4130–4133.
(10) Addamo, M.; Augugliaro, V.; Di Paola, A.; Garcia-Lopez, E.; Loddo, V.; Marci, G.; Molinari, R.; Palmisano, L.; Schiavello, M. *J. Phys. Chem. B* **2004**, *108* (10), 3303–3310.
(11) Matijevic, E. *Langmuir* **1986**, *2*, 12–20.
(12) Siegal, R. W. *Sci. Am.* **1996**, *275*, 74–70.
(13) Gerko, O.; Zeshan, H.; Penn, R. L.; Pesika, N.; Searson, P. C. *Phys. Rev. E.* **2002**, *66*, 011403–1to 0011403–4.
(14) Greenwood, G. W. *Acta Metall.* **1956**, *4*, 243–248.
(15) Lifshitz, I. M.; Slyozov, V. V. *J. Phys. Chem. Solids* **1961**, *19*, 35–50.
(16) Penn, R. L.; Banfield, J. F. *Geochim. Cosmochim. Acta* **1999**, *63* (10), 1549–1557.
(17) Leite, E. R.; Giraldi, T. R.; Pontes, F. M.; Longo, E. *Appl. Phys. Lett.* **2003**, *83* (8), 1566–1568.

10.1021/cm071057o CCC: $40.75
Published on Web 05/06/2008

et al. and Penn et al.,[18,19] in CoOOH by Penn et al., [19] in Fe_2O_3 by Penn et al.,[19] in ZnO by Gerko et al., [13] and ZnS by Ocaña et al. and Huang et al.[20,21] Evidence of OA has also been demonstrated in PbSe by Cho et al., [22] in ZnWO4 by Liu et al.,[23] in CuO by Lie et al., [24] in $BiPO_4$ by Geng et al.,[25] in CdTe by Tang et al., [26] in ZrO2 by I-Ming et al.,[27] and in PbS by Zhang et al.[28] In the literature are also detailed descriptions of the mechanisms of growth via OA.[29–31]

It is significant that many of the materials that have been observed to grow by OA are relatively insoluble. As the rate of OR is proportional to the aqueous ion concentration, the relative importance of OA is likely to be enhanced when dissolution is limited. Both mechanisms may operate simultaneously, with the dominant pathway changing with solution chemistry, particle surface condition, and temperature.[21] The balance of growth pathways will affect the coarsening rates and product morphology.

Both OA and OR are well-documented growth mechanisms, but never has the role of environmental conditions on the predominance of each been clearly laid out in nanoparticle colloids. Therefore, a systematic study of these phenomena under a range of pH and temperature was carried out. Not only could this provide information relevant to predicting the evolution of geochemical systems and engineering devices, but it will also help outline clear routes to a desired size and morphology for use in engineering devices. Furthermore, the role of surface energy and solubility on anatase growth was elucidated by monitoring its development under different pH and temperature with SEM, TEM, and XRD. The principle relating environmental condition to surface characteristics and, in turn, growth behavior brought forth here could be applied to other oxide nanoparticle systems leading the way to greater understanding of natural colloidal systems and greater control of devices incorporating nanotechnology.

Experimental Section

Nanocrystalline titania was synthesized by the sol–gel method. A volume of 2.25 L deionized (DI) water was used as a solvent for synthesis and its pH was adjusted to 1.10 with 12 M HCl. The solution was cooled to 4–6 °C in an ice bath. Then a solution containing 22.5 mL of titanium(IV) isopropoxide ($Ti[OCH(CH_3)_2]_4$) and 225 mL of ethanol was slowly dripped into the solvent undergoing magnetic stirring.

Titania precipitated from the solution as the liquid was evaporated in an 80 °C oven. The obtained titania powder was then reintroduced into 100 mL DI water, forming a colloidal suspension with a pH of 2.05. Ions adsorbed on colloid particles were removed by dialysis. The titania colloid suspension was put into a dialysis tube made of a Spectra/Por (molecular weight cut off (MWCO) of 3500 Daltons) membrane and placed into a DI water bath under slow magnetic stirring. After the water in the bath was changed four times over the period of about 2 days, the colloid formed a gel, indicating that the pH of the colloid had risen to near the zero point of charge of the titania. The measured pH of the colloid in the dialysis tube and that of the water in the bath were both 5.2. This value is in agreement with the pH_{PZC} (pH at the point of zero net proton charge) of titania determined experimentally by numerous researchers.[32–39] The dialyzed titania was dried for two days at 30 °C, yielding ~3 g of titania powder. The powder was further evacuated for one day using a Micromeritics ASAP 2010 gas adsorption instrument under a vacuum of 3 μm Hg pressure, and then stored in a desiccator.

The samples were characterized by powder X-ray diffraction (XRD). About 0.5 mg of titania powder was dispersed with ethanol and then transferred to a low-background single-crystal quartz plate for diffraction analysis. XRD patterns were collected using a Bruker Baker diffractometer (Cobalt target, 45 mV, 35 mA) in a 2θ range of 24−68° with a step size of 0.01° and a dwell time of 1 s at each step. After fitting the Pearson VII functions to chosen XRD peaks, the full width at the half-maximum (fwhm) of each peak was obtained after correction for instrumental broadening. The particle sizes of titania particles were calculated from the fwhm data using the Scherrer equation with a Scherrer constant of 0.9.

The integrated areas of rutile 110, brookite 121, and anatase 101 peaks were used to calculate the phase content in a sample after hydrothermal treatment using an analytical method developed previously.[40] The as-synthesized nanoparticles were also examined with an ARM high-resolution transmission electron microscope (TEM) operated at 800 KV and a TopCon O2B 200 KV TEM. A small drop of a powder-ethanol suspension was placed on a Formvar-coated copper grid and the size, size distribution, morphology, and crystallinity were determined.

Hydrothermal growth experiments were carried out in Teflon cups enclosed in general purpose acid digestion bombs (Parr Instrument Co.). Approximately 30 mg of the as-synthesized titania sample were put into a Teflon cup containing 9 mL of DI water. The pH of the suspension in the cup was adjusted to a target value (i.e., 1–12) with HCl or NaOH. After the suspension was sonicated for 15 min, the assembled bomb was put into an electric furnace

(18) Banfield, J. F.; Welch, S. A.; Zhang, H. Z.; Thomsen, E. T.; Penn, R. L. *Science* **2000**, *289*, 751–754.
(19) Penn, R. L.; Oskam, G.; Strathmann, T. J.; Searson, P. C.; Stone, A. T.; Veblen, D. R. *J. Phys. Chem. B* **2001**, *105*, 177–2182.
(20) Ocaña, M.; Morales, M. P.; Serna, C. J. *J. Colloid Interface Sci.* **1995**, *171* (1), 85–91.
(21) Huang, F.; Zhang, H. Z.; Banfield, J. F. *Nano Lett.* **2003**, *3* (3), 373–378.
(22) Cho, K. S.; Talapin, D. V.; Gaschler, W.; Murray, C. B. *J. Am. Chem. Soc.* **2005**, *127*, 7140.
(23) Liu, B.; Yu, S. H.; Li, L.; Zhang, F.; Zhang, Q.; Yoshimura, M.; Shen, P. *J. Phys. Chem. B* **2004**, *108* (9), 2788–2792.
(24) Liu, B.; Zeng, H. C. *J. Am. Chem. Soc.* **2004**, *126* (26), 8124–8125.
(25) Geng, J.; Hou, W. H.; Lv, Y. N.; Zhu, J. J.; Chen, H. Y. *Inorg. Chem.* **2005**, *44* (23), 8503–8509.
(26) Tang, Z.; Kotov, N. A.; Giersig, M. *Science* **2002**, *297* (5579), 237–240.
(27) Chena, I. M.; Yeha, S. W.; Chiou, S. Y.; Gan, D. S.; Shen, P. Y. *Thin Solid Films* **2005**, *491* (22), 339–346.
(28) Zhang, W. Q.; Yang, Q.; Xu, L. Q.; Yu, W. C.; Qian, Y. T. *Mater. Lett.* **2005**, *59* (27), 3383–3388.
(29) Niederberger, M.; Cölfen, H. *Phys. Chem. Chem. Phys.* **2006**, *8*, 3271–3287.
(30) Cölfen, H.; Mann, S. *Angew Chem., Int. Ed.* **2003**, *42* (21), 2350–2365.
(31) Cölfen, H.; Antonietti, M. *Angew. Chem., Int. Ed.* **2005**, *44* (35), 5576–5591.
(32) Noh, J. S.; Schwarz, J. A. *J. Colloid Interface Sci.* **1989**, *130* (1), 157–164.
(33) Parks, G. A.; De Bruyn, P. L. *J. Phys. Chem.* **1962**, *66*, 967–972.
(34) Yoon, R. H.; Salman, T.; Donnay, G. *J. Colloid Interface Sci.* **1979**, *70* (3), 483–493.
(35) Sverjensky, D. A. *Geochim. Cosmochim. Acta* **1994**, *58* (14), 3123–3129.
(36) Rodriguez, R.; Blesa, M. A.; Regazzoni, A. E. *J. Colloid Interface Sci.* **1996**, *177*, 122.
(37) Spanos, N.; Georgiadou, I.; Lycourghiotis, A. *J. Colloid Interface Sci.* **1995**, *172*, 374.
(38) Bourikas, K.; Hiemstra, T.; Van Riemsdijk, W. H. *Langmuir.* **2001**, *17* (3), 749–756.
(39) Machesky, M. L.; Wesolowski, D. J.; Palmer, D. A.; Ichiro-Hayashi, K. *J. Colloid Interface Sci.* **1998**, *200* (2), 298–309.
(40) Gribb, A. A.; Banfield, J. F. *Am. Mineral.* **1997**, *82*, 717–728.

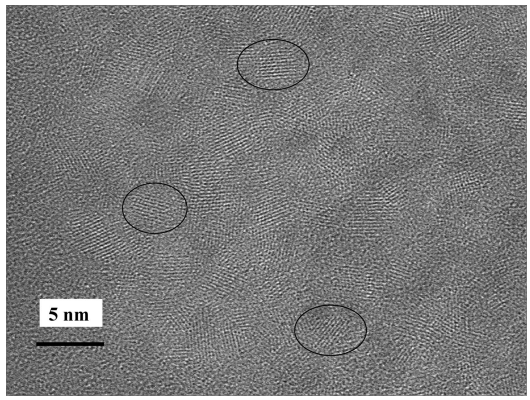

Figure 1. TEM image of anatase nanoparticles synthesized by hydrolysis of titanium isopropoxide at 5 °C and pH 1. Individual particles less than 4 nm are circled.

held at 105, 200, or 250 °C for a required time. The bomb was removed from the furnace and cooled in air. The pH of the suspension was determined again.

The extent and nature of coarsening and morphology development were monitored by XRD and TEM, as described for characterization of the as-synthesized particles. High-resolution scanning electron microscope (SEM) images obtained using a Hitachi S-5000 were also used to determine size, morphology, and aggregation state and to clarify the coarsening mechanism of the anatase nanoparticles.

Results

The anatase α peak was chosen for anatase size determination of the synthesized materials because it was the only peak with a high enough XRD intensity for size analysis. The length was determined using an analytical method developed previously.[41] The average particle size of the as-synthesized anatase determined from XRD peak broadening is 3.5 nm. This is in good agreement with the average size determined by atomic resolution TEM imaging (Figure 1). TEM data also show that the 3.5 nm particles are near-spherical.

The as-synthesized titania sample contained ~85% anatase and ~15% brookite. The size and morphology of the as-synthesized brookite particles are difficult to accurately determine because the brookite peaks are very small. However, based on peak broadening, we estimate that the average diameter of brookite is 3–5 nm.

The coarsening of anatase is recorded in Figures 2–4. The average diameter of anatase measured normal to {101} is plotted as a function of time at temperatures of 105, 200, and 250 °C in solutions of different pH. The average diameter was determined via Scherrer analysis for all of the data in Figure 2. In Figure 3, Scherrer analysis was used for all the data except for the sample coarsened in high pH conditions (light blue) and in Figure 4, SEM image analysis was used exclusively for determining particle diameter.

At 105 °C, coarsening rates are relatively pH independent from pH 1 to pH 8. The coarsening rate is slightly higher at pH 11.5. At 200 °C, the coarsening rates are pH independent from pH 1.0 to 8.1 and increase dramatically at pH 11.5,

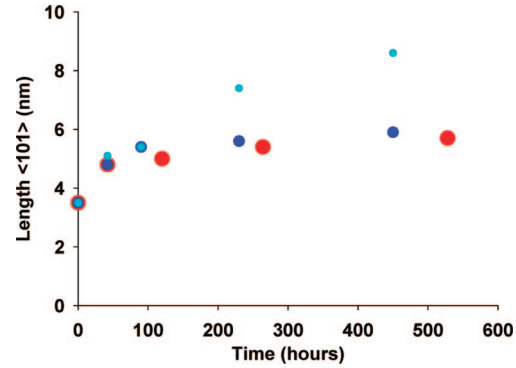

Figure 2. Anatase α length as a function of hydrothermal treatment time at 105 °C. The red points are at pH 1, blue are at pH 8, light blue are at pH 11.5.

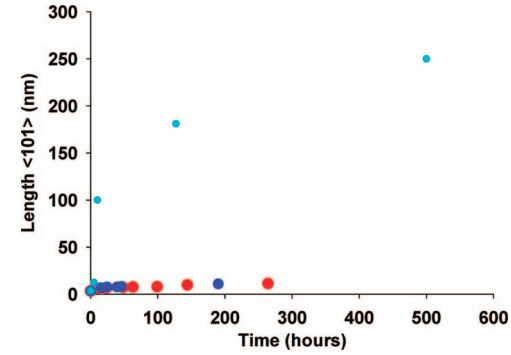

Figure 3. Anatase α length as a function of hydrothermal treatment time at 200 °C. The red points are at pH 1, blue are at pH 6.5, and light blue are at pH 11.5.

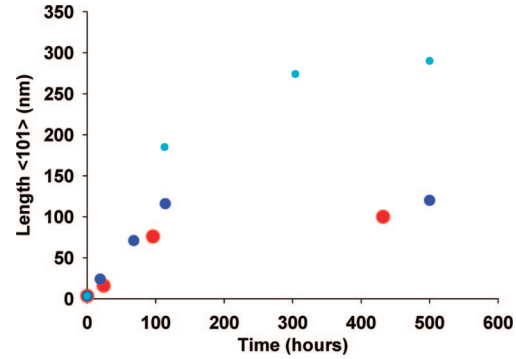

Figure 4. Anatase α length as a function of hydrothermal treatment time at 250 °C. The red points are at pH 2.1, blue are at pH 8.5, and light blue are at pH 11.5.

where there is rapid growth from 3.5 nm to greater than 150 nm within 150 h. At 250 °C, the rate of crystal growth is pH-independent at pH values 4–9, with an average particle size of about 100 nm after 200 h. At pH 11.5 particles grow to almost 200 nm within 200 h. Below pH 4 at 250 °C, the anatase growth rate is meaningless because it is rapidly transforming to rutile, so size measurements reflect the balance of two competing processes (dissolution and coarsening).

Information about particle size, morphology, particle–particle arrangements, and growth rates deduced from TEM and SEM images at various pH's, coarsening times, and temperatures are shown in Figures 5–11. The images, along with the kinetic data, help to uncover information about growth mechanisms occurring in each solution condition.

(41) Zhang, H. Z.; Banfield, J. F. *J. Phys. Chem. B* **2000**, *104* (15), 3481–3487.

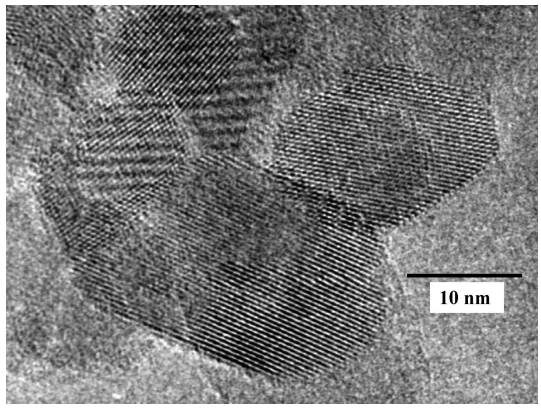

Figure 5. TEM image of anatase nanoparticles coarsened for 127 h at pH 12 and 200°. The particle in the lower part of the image has morphology close to the predicted tetragonal bipyramid morphology of anatase where {101} faces are exposed; {100} faces are also exposed. The crystal on the upper-right side of this image is viewed down the [100] and shows the dominance of {101} surfaces with clear (001) terminations.

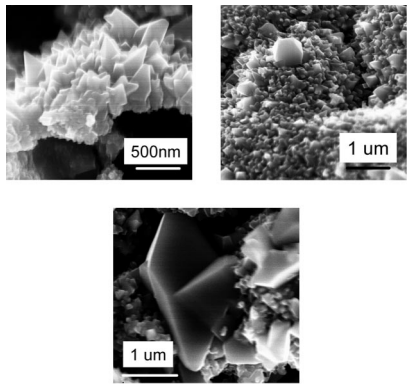

Figure 6. SEM images of anatase nanoparticles coarsened for 127 h at pH 11.5 and 200°.

200 °C, pH 11.5. Figure 5 is an HRTEM image that shows anatase crystals coarsened in pH 11.5 for 127 h at 200 °C. The anatase crystals have lengths between 10 and 20 nm. The crystal on the upper-right side of this image is viewed down the [100] and shows dominance of {101} surfaces with clear (001) terminations. SEM images of the same sample shows anatase crystals with well developed morphology and an average size of 181 nm (Figure 6), surrounded by many smaller, aggregated anatase crystals. Image analysis of Figure 6 reveals a particle size distribution that is irregular with most particles between 50 and 150 nm in length. There are several much larger particles but these outliers are not clustered around any particular length yielding a distinct bimodal distribution. Rather, the frequency of larger particles taper off as a function of size (see the Supporting Information). The well-defined shapes in Figures 5 and 6 and broad size distribution of anatase are consistent with growth via OR.

200 °C, pH 5. The image in Figure 7 shows a TEM image of anatase crystals hydrothermally coarsened in pH 5 for 16 h at 200 °C. The nanoparticles have attached and share a common crystallographic orientation. The SEM image in Figure 8 shows that particles coarsened under these conditions have adopted rodlike shapes as well as {101}-based morphologies similar to those shown in Figures 5 and 6.

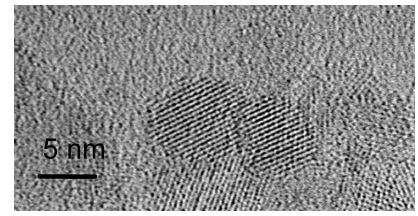

Figure 7. TEM image of particles attaching. They have been hydrothermally treated for 16 h at pH 5 and 200 °C. One set of {101} type lattice fringes are coherent.

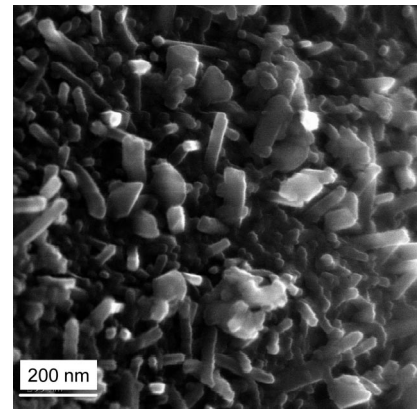

Figure 8. SEM image of titania hydrothermally coarsened for 144 h at pH 5 and 200 °C. Both elongated rods and bipyramidal tetrahedrons are exhibited on the surface of the aggregate.

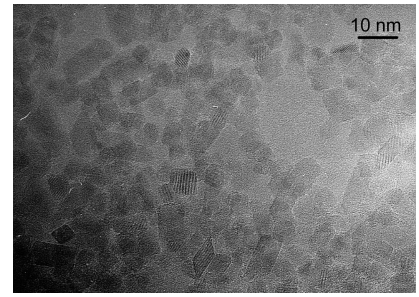

Figure 9. TEM image of titania hydrothermally coarsened for 144 h at pH 1 and 200 °C.

200 °C, pH 1. A TEM image of titania crystals coarsened under acidic conditions is shown in Figure 9. Elongated crystals, irregularly shaped crystals, and crystals that have attached can all be seen in the Figure.

250 °C, pH 11.5. As mentioned above, at 250 °C the plot in Figure 4 shows a rapid decline in coarsening rate from samples in a pH 11.5 solution to those in a lower pH solution. An SEM image of a sample coarsened at 250 °C, pH 11.5 for 114 h (Figure 10) shows a wide particle size distribution (see the Supporting Information) with an average size of about 147 nm. Furthermore, the sample contains several very well formed {101}- based tetragonal bipyramids.

250 °C, pH 5.3. Figure 11 shows a sample coarsened for 96 h at pH 5.3 at the same temperature. The average particle diameter in this sample is $\sim$ 80 nm and some nonequilibrium morphology particles are evident. However, the amount of particles with nonequilibrium morphology is less than in samples coarsened at similar times and the same pH at 200 °C.

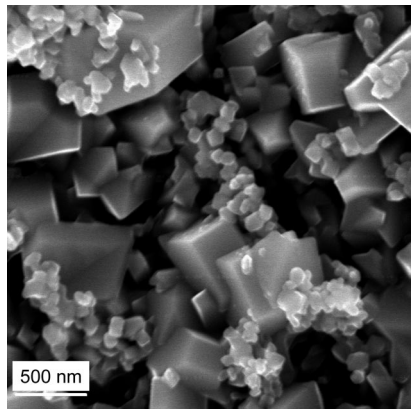

Figure 10. SEM image of titania hydrothermally coarsened for 114 h at pH 11.5 and 250 °C.

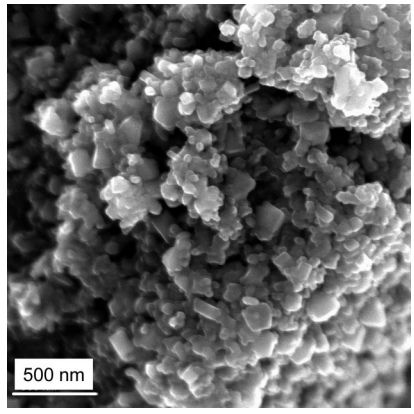

Figure 11. SEM image of titania hydrothermally coarsened for 96 h at pH 5.3 and 250 °C.

Discussion

Fitted growth rates can be compared with Ostwald ripening and oriented attachment models, which have different mathematical forms, to help determine which one dominates at a particular pH. Ostwald ripening of individual crystals of average particle diameter, d, dispersed in a homogeneous matrix can be described by the following equation[15,42]

$$d^n = d_o^n + kt \quad (1)$$

where d_o is the initial average diameter, k is a temperature-dependent constant, and t is time. The exponent, n, is related to the mode of Ostwald ripening. When n is 2, crystal growth is controlled by attachment of ions along the matrix-particle boundary, when $n = 3$, the growth is controlled by the volume diffusion of ions in the matrix, and when $n = 4$, grain boundary diffusion control growth.[15,42] The temperature-dependent constant, k, is appropriate to the value of the exponent n.[43] When $n = 3$, the expression for k is

$$k = 8\gamma V^2 c/54\pi\eta a N_a \quad (2)$$

where γ is the interfacial surface tension, V is molar volume, c is the Ti solubility, η is the viscosity of the solution, a is the solvated ion radius, and N_a is Avogadro's number.[13]

When the constant, n, is set to 2, 3, 4, and beyond and the diameter to the power of n is plotted as a function of t, the goodness of fit of coarsening data to the linear form of eq 1 can be ascertained. The goodness of fit (r^2 value) of all of the data sets for the hydrothermal coarsening runs for multiple values of n are tabulated in the Supporting Information. At 105 °C, there is very poor linear fit at $n = 2$, 3, or 4 for samples coarsened at a low or middle values of pH. At pH 11.5, the data points become linear when n is set to 3 having an r^2 value of 0.99. At 200 °C, there is very poor linear fit at $n = 2$, 3, or 4 for samples coarsened at low and middle values of pH. At pH 11.5, the data points become linear when n is set to 3 having an r^2 value of 0.98. The same is true for samples coarsened at 250 °C. Below pH 8.5, the data cannot be fit because of transformation to rutile. There is very poor linear fit at pH 8.5. At pH 11.5, the data becomes linear at $n = 3$ and higher.

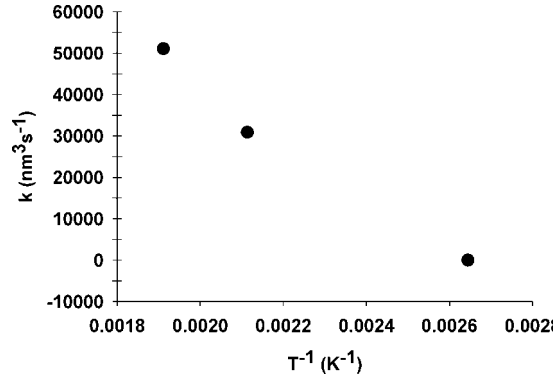

Figure 12. Temperature-dependent constant, k, as a function of the inverse of temperature for the samples coarsened at pH 11.5 and that fit to eq 1.

The linear dependence is evidence that growth at very high pH, where solubility is 2 orders of magnitude higher, proceeds by Ostwald ripening and is rate limited by the volume diffusion of ions in the matrix. The fact that samples coarsened near the pH_{PZC} or lower do not fit the linear for eq 1 suggests that Ostwald ripening alone cannot explain the coarsening mechanism of these samples.

The temperature dependent constant, k, is plotted as a function of the inverse of temperature for the samples coarsened at pH 11.5 and that fit to eq 1 in Figure 12. The constant increases by over 4 orders of magnitude over the temperature range 105 to 200 °C (from $k = 1.3$ to $k = 30\,895$) and increases by a factor of 1.65 from 200 to 250 °C (from $k = 30\,895$ to $k = 51\,082$). The physical parameters that can explain this dependence are γ, V, c, η, and a, depicted in eq 2.

The temperature dependence of the molar volume, V, is expected to be very weak in this temperature range because the thermal expansion coefficient of TiO_2 is very small. Similarly, the solvated ion radius, a, is not expected to vary significantly with temperature. The viscosity of water does increase with temperature but not significantly.[44]

Regarding the phenomena of dissolution, the relevant components of surface energy, γ, are the electrostatic energy of adsorbed ions and the interfacial tension. However, at a solution pH far from the pH_{PZC}, the contribution of the

(42) Wagner, C. *Z. Elektrochem.* **1961**, *65*, 581–591.
(43) Sun, W. *Acta. Mater.* **2005**, *53*, 3329–3334.
(44) Oskam, O.; Nellore, A.; Penn, R. L.; Searson, P. C. *J. Phys. Chem. B* **2003**, *107* (8), 1734–1738.

adsorbed ions dominants the overall surface energy.[45] Thus, the behavior of adsorbed ions as a function of temperature should help explain the increase in the constant, k, of eq 2. Indeed, Machesky et al. experimentally demonstrated that negative surface charge, above the pH_{PZC}, does increase with increasing temperature.[46]

The solubility of titania is not only dependent on pH, increasing about 3 orders of magnitude from the pH_{PZC} to pH of 11.5, but it also increases between two and 3 orders of magnitude at pH 11.5 from 100 to 200 °C. Also, there is a slight increase in the solubility from 200 to 250 °C.[47,48] This large increase from 100 to 200 °C and smaller increase from 200 to 250 °C directly corresponds with the k values experimentally determined here.

Other than these three samples at pH 11.5, the average particle size of the hydrothermally coarsened samples do not fit the Ostwald ripening equation. Thus, some other growth mechanism must be playing a role.

Morphological evolution can yield clues to the dominating crystal growth pathway. The equilibrium morphology of anatase is an octahedron (tetragonal bipyramid) terminated by {011} that may be capped by {001}.[49] Growth by Ostwald ripening yields this equilibrium morphology predicted by Wulff's theorem, which states that the sum of the product of the facet energies and facet areas is a minimum,[34] because the atoms in the solution have enough thermal energy to overcome kinetic barriers to equilibrium growth. On the other hand, particles that show evidence of an attaching event or assume irregular shapes that could only occur after an attachment event is a clue that OA is the coarsening mechanism. In evaluating evidence for OR- vs OA-based growth, we consider the following: (i) evidence for oriented fused nanoparticles, indicative of OA; (ii) presence of a large and smoothly varying particle size distribution, consistent with OR; (iii) presence of large crystals with equilibrium morphology, consistent with OR; (iv) elevated growth rates at high Ti solubility conditions (dependent primarily on pH), likely indicative of OR; (v) kinetic data fits Ostwald ripening equation as discussed above.

On the basis of these criteria verified with XRD, TEM, and SEM analyses, we identify three distinct coarsening pathways for anatase — Ostwald ripening at high pH, a combination of Ostwald ripening and oriented attachment pH near pH_{PZC}, and a combination of Ostwald ripening, oriented attachment and dissolution and regrowth as rutile at low pH. At pH >11, coarsening proceeds exclusively via Ostwald ripening. In these solutions, there is no direct evidence for growth via OA at any temperature. Fitting to the Ostwald ripening equation and analysis of TEM and SEM data which show wide particle size distribution (see the Supporting Information), equilibrium morphologies, and elevated growth rates, indicate criteria which suggest that growth at high pH occurs via OR. Thus, we conclude that at pH >11, OR dominates because the solubility of Ti is 3 orders of magnitude higher than at the pH_{PZC}[34] and the high interfacial electrostatic potential blocks particle–particle interactions required for growth via OA and induces a higher surface energy, which is conducive for Ostwald ripening.

The second growth pathway occurs over the pH range 2−11, where both OR and OA occur simultaneously. We attempted to fit the data to a model devised by Huang et al. to describe growth of ZnS solely by OA and it turned out the data cannot be describe with that model. This model assumes particle volume doubles after OA events and that OA-based growth is related to the number of particles in a given volume.[21] As stated above, the data does not fit the OR model either. Therefore, growth is not occurring solely via OA or OR. Both pathways may be contributing to growth under these conditions.

TEM data can also provide clear evidence for growth via OA. An image of nanoparticles demonstrating this is shown in Figure 7 (coarsened at pH 5). This process results in asymmetrical morphology, as observed in Figure 8 (pH 5). Thus, criteria (i) and (iii) support the conclusion that OA is occurring over much of the pH range.

Thus, we conclude that this second growth pathway is characteristic of OR and OA contributing simultaneously. This occurs at pH values on either side of the pH ZPC, where OR is less favored because of low Ti solubility. The electrostatic repulsion is lower close to the pH ZPC, allowing nanoparticles to contact each other during the course of random motion. Particles may attach on coherent crystallographic planes or approach and rotate until coherence is obtained.

There is a third coarsening pathway observed at low pH, in which there is SEM and TEM evidence for growth by both OA and OR. However, under these conditions, anatase growth occurs in parallel with nucleation and growth of rutile at 200 and 250 °C. Rutile is the stable phase for bulk TiO_2 under most temperature and pressure conditions. However, anatase is stabilized relative to rutile at small particle sizes,[50] except at low pH, where the relative surface energies are modified by proton adsorption.[45] When smaller particles of anatase are present, their dissolution protects the largest anatase particles from dissolving. Consequently, anatase appears to grow early in the experiments at a rate that is similar to that observed over most of the pH range. However, eventually, all anatase dissolves to form rutile (the loss of the few remaining large anatase particles cannot be observed because the abundance of anatase is too low at this stage). The amount of transformation as a function of time and temperature is quantified in detail in another publication.[45] The lack of rutile formation at 100 °C is attributed to sluggish transformation kinetics.[51]

(45) Finnegan, M. F.; Zhang, H. Z.; Banfield, J. F. *J. of Phys. Chem. C* **2007**, *111*, 1962–1968.
(46) Machesky, M. L.; Palmer, D. A.; Wesolowski, D. J. *Geochim. Cosmochim. Acta* **1994**, *58* (24), 5627–5632.
(47) Knauss, K. G.; Dibley, M. J.; Bourcier, W. L.; Shaw, H. F. *App. Geochem.* **2001**, *16*, 1115–1128.
(48) Schmidt, J.; Vogelsberger, W. *J. Phys. Chem. B* **2006**, *110*, 3955–3963.
(49) Oliver, P. M.; Watson, G. W.; Kelsey, E. T.; Parker, S. C. *J. Mater. Chem.* **1997**, *7* (3), 563–568.
(50) Zhang, H. Z.; Banfield, J. F. *J. Mater. Chem.* **1998**, *8* (9), 2073–2076.
(51) Madras, G.; McCoy, B. J.; Navrotsky, A. *J. Am. Ceram. Soc.* **2007**, *90* (1), 250–255.

The coarsening kinetics, described by the data in Figures 3 and 4, reveal an aspect of the OA growth pathway. The data show the degree of rate increase at pH 11.5 at 200 °C is much higher than that for anatase coarsening at 250 and at 105 °C. This result suggests that, in extreme basic solution, OA is less inhibited as the temperature decreases from 250 to 200 °C. At 250 °C, although particle impingement rates are higher, attachment rates may be lower than that at 200 °C because particle kinetic energies are too high. In other words, thermal energy suppresses OA because rapid particle motion decreases the probability of particle–particle attachment, thus explaining why the coarsening rate increase is much higher above pH 11 at 200 than at 250 °C. However, at 105°, the rate increase is very subtle because of a very small rise in OR rate. Even though Ti solubility increases as pH rises to very high values, a sluggish dissolution rate and atomic diffusion rate limit the rate increase.

Supporting Information Available: Particle size distribution and goodness of fit data (PDF). This material is available free of charge via the Internet at http://pubs.acs.org.

CM071057O